Proceedings of the ASME 2016 TURBO EXPO &
Turbomachinery Technical Conference & Exposition
GT 2016
June 13-17, 2016, Seoul, SOUTH KOREA

GT2016-57968

DETAILED NUMERICAL STUDY OF FLOW AND VORTEX DYNAMICS IN STAGGERED PIN-FIN ARRAYS WITHIN A CHANNEL

K. Kannan[*], M. Khoshlessan
School for Enginnering of Matter, Transport
& Energy(SEMTE)
Arizona State University
Tempe, AZ 85281
Email: kkannan4@asu.edu
Email: mkhoshle@asu.edu

M. Herrmann, Y. Peet
School for Enginnering of Matter, Transport
& Energy(SEMTE)
Arizona State University
Tempe, AZ 85281
Email: marcus.herrmann@asu.edu
Email: ypeet@asu.edu

ABSTRACT

Pin-fin arrays are known to enhance heat transfer from heated surfaces and provide important industrial applications such as increasing internal heat transfer to a turbine blade or solar receiver. Several studies on heat transfer characteristics of various pin-fin arrangements and effects of geometrical parameters on heat transfer have been performed in the past. The present paper aims to address main aspects of fluid flow and heat transfer interactions through a pin-fin array with the help of high-fidelity numerical simulations and focuses on three issues. The first one is to evaluate the effect of three dimensional flow physics such as horseshoe vortices and periodic unsteadiness from vortex shedding on the spatial variation of heat transfer. The second target is to analyze the effect of free end clearance in the case of finite height pin-fin arrays with added flow complexity relative to wall-bounded pin-fin arrays, to provide a comprehensive picture of the flow physics introduced by free ends. The third one is to provide a general guideline for the numerical simulation of flows through pin-fin arrays by comparing simulations on reduced span-wise domains with the full multi-row pin configuration, to elucidate the significance of wall effects. In addition, comparison of the flow characteristics in different stream-wise row locations, is performed to establish the domain length where self-similarity might occur with inflow/outflow conditions. All simulations are conducted for low Mach number incompressible flow with temperature as a passive scalar. The current formulation assumes that variations in temperature have no effect on the fluid motion by choosing appropriate thermal boundary conditions that are still within the realistic parameter range for turbine cooling. In this paper, we perform flow simulations using the Large Eddy Simulation methodology. Two numerical codes, one based on a Finite Volume method and the other based on a Spectral Element approach, are benchmarked with each other and validated versus experiments available in the literature (Ostanek and Thole, 2012).

NOMENCLATURE

C_s	Smagorinsky constant
D	Pin Diameter
D_H	Hydraulic Diameter
e	Relative error compared to the experiment
f	Frequency of vortex shedding
FVM	Finite Volume Method
H	Channel height, Pin-fin height
$\frac{L_r}{D}$	Wake closure position, location of zero mean stream-wise velocity along the wake axis
Pr_{SGS}	Sub-grid scale Prandtl number
q''	Heat flux
Re_D	Pin-fin Reynolds number, $Re_D = U_{max} D \nu^{-1}$
Re_{DH}	Pin-fin hydraulic Reynolds number, $Re_{DH} = U_m D_H \nu^{-1}$

---

[*] Correspondence author: K. Kannan

Re_H	Channel Reynolds number, $Re_H = U_m H \nu^{-1}$
St	Strouhal number, $St = \frac{fD}{U_{max}}$
SEM	Spectral Element Method
T	Temperature
U_m	Bulk velocity
U_{max}	Average velocity through minimum flow area
U, V, W	Instantaneous stream-wise, transverse and span-wise velocity components
x	Stream-wise distance
y	Transverse distance
y^+	Dimensionless transverse distance from wall, $y^+ = U_\tau y \nu^{-1}$
z	Span-wise distance

Greek Letters

ν	Molecular kinematic viscosity
ν_t	Turbulent kinematic viscosity
λ_2	Lambda vortex
Δt	Non-dimensional time step, $\Delta t = \frac{tU_m}{D}$

INTRODUCTION

Flow over pin-fin arrays mounted on a wall is of considerable practical interest in fluid mechanics. It has numerous applications such as heat exchangers in gas turbine airfoils, nuclear power plants, boilers and directly irradiated volumetric receivers. The operating principle is based on air being forced through the array and energy transport takes place to the working fluid flowing within and over the array via heat convection. Because of the wide range of applications, prediction of the energy transport capability along each pin and effects of their interaction, rate of convective heat transfer between the pin surface and the working fluid, and temperature distribution through the array are of great importance for designing more efficient and reliable pin-fin configurations. The considerable fundamental interest in flow through pin-fin arrays is due to a highly unsteady and three dimensional nature of the flow and various interacting vortex systems. One of these interacting vortex systems is the horseshoe vortex (HV) which is present at the pin-fin and end-wall junction. There is also another vortex system known as Von-Karman vortex (KV). Earlier studies on the dynamics of horseshoe vortex systems have shown that they include a primary horseshoe vortex (HV), a secondary vortex upstream of the horseshoe vortex (SV), a tertiary vortex upstream of the secondary vortex (TV), and a small vortex in the corner region of the junction (CV) (Hunt et al. [1] Praisner et al. [2]). There have been a wide range of studies on the time mean and instantaneous flow, and on the mechanisms that give rise to an increase in the end-wall heat transfer of a body end-wall junction. Ames et al. [3] performed a detailed study of the end-wall heat transfer distributions in a staggered pin-fin array using an infrared camera at Reynolds numbers of 3000, 10000, 30000. Their detailed heat transfer distributions highlighted the influence of the horseshoe vortex system in the entrance region on the end-wall heat transfer and the wake generated turbulence throughout the pin-fin array. Ostanek [4] made more detailed flow field and heat transfer measurements for an array of staggered pin-fins. He showed that, for low Reynolds numbers, average heat transfer was dominated by the horseshoe vortex in the initial row. In the downstream rows, however, the horseshoe was not as distinguished as in the first row. In another work, Ostanek and Thole [5] performed a detailed isothermal experimental study on the effect of stream-wise spacing on the near wake. The stream-wise spacing was varied between 3.46D and 1.73D and experiments were conducted at Reynolds numbers of 3000 and 20000. Their results showed that the vortex shedding frequency increases for decreasing stream-wise spacing. Moreover, in the third pin-fin row, the wake closure position was reduced to a greater extent than in the first row wake due to the generated turbulence in the upstream rows. The level of turbulent kinetic energy also decreased for decreasing stream-wise spacing. Ames and Dvorak [6] investigated the pin-fin midline heat transfer. They used hot wire anemometry to acquire turbulence measurements and velocity distributions at three Reynolds numbers of 3000, 10000, 30000. Their results showed that heat transfer augmentation due to turbulence is highest in row 4 and beyond. Delibra et al. [7] used large eddy simulation coupled with a URANS treatment to compute the flow and heat transfer in a matrix of staggered, cylindrical, thermally passive pins bounded by heated end-walls at two Reynolds numbers of 10000 and 30000. According to their results, large scale coherent vortical structures are the general mechanisms for heat removal from the end-walls. They showed that large vortex systems are the dominant heat transfer modes away from the end-wall. These results are consistent with what has been previously reported in [6]. If free ends are present, the free ends also add to these flow complexities and the vortices being shed from the free end interact with the vortex shedding from the cylinder surface [8]. Sparrow and Ramsey [9] performed mass transfer experiment on a staggered array of circular cylinders situated in a cross-flow of air in a flat rectangular duct. According to their experiments, tip clearance gives rise to a transverse flow component superposed on the main flow that passes around the circumference and as a result, the wake flow is strongly three dimensional. The fully developed heat transfer coefficients were quite insensitive to a cylinder height (or extent of tip clearance). The effect of tip clearance on the performance of the heat transfer and pressure drop at low Reynolds number was investigated through numerical and experimental studies by Deqing et al. [10]. According to their results, the heat transfer and pressure drop performance in the case of low Reynolds number is quite sensitive to the tip clearance, and the introduced tip clearance can enhance the heat transfer and reduce the pressure drop effectively. Moores and Joshi [11] experimentally evaluated the effect of tip clearance on a liquid cooled array of shrouded pin-fins. Three arrays of height to diameter ratios ranging from 0.5 to 1.1 and tip clearance of 0 to 25% of pin height were evaluated. Increased mean heat transfer and lower overall pressure drop were realized for clearances of less than 10%. The increase in heat transfer was attributed to the additional surface area when clearance was introduced. However, they showed that the heat transfer efficiency of the fin at the tip is lower compared to the array as a whole. According to other studies [12]- [13], tip clearance results in two competing effects. The first is the promotion of the heat transfer rate due to the increase in the heat transfer coefficient at the tip surface. The second is the restraint of the heat transfer rate due to the effect of flow bypass. In the present study two different numerical approaches are employed to perform large eddy simulation of flow over staggered arrays of cylindrical, thermally active pins bounded by heated end-walls. Considered is a Reynolds number of 3000, based on the pin diameter and velocity through the minimum flow area. In the first part of the present study, the two numerical methods are validated against the isothermal experiments of Ostanek and Thole [5]. In the second part, a second geometry based on the geometry in [5] is defined with a free space of $1D$ above the pins. A detailed study of the flow field, the complex flow structures, and a comparison of the flow topology with the full height case provides a comprehensive picture of the complex flow behavior. The data at different locations are analyzed and compared between the two geometries which may allow for further optimization of pin-fin configurations.

NUMERICAL SOLUTION PROCEDURE

In the current paper, we use two different numerical approaches: a Spectral Element Method (SEM), and a Finite Volume Method (FVM), both employing the Large-Eddy Simulation (LES) methodology. The reason is to provide a higher level of confidence and reduce uncertainty in results, especially where experimental data is not easily available. It should be noted that the present study does not aim to determine which code is better. The Navier-Stokes equations are solved under the low Mach number, incompressible approximation, where thermodynamic variables, such as density and temperature, are assumed to be decoupled from variations in pressure. The two numerical approaches are described in the following sections:

1. Spectral Element Method (SEM)

In the Spectral Element Method, the implicitly filtered incompressible Navier-Stokes equations with advective temperature scalar are being solved. The LES sub-grid scale model used is the standard Smagorinsky model with low pass spectral filtering. The parameter C_s in the eddy viscosity ν_t and sub-grid scale Prandtl number Pr_{SGS} are assumed to be 0.1 and 0.85 respectively. The code is based on the spectral element solver Nek5000 [14]. A non-dimentional time step of $\Delta t = 0.1e-3$ was used to obtain fully converged results.

2. Finite Volume Method (FVM)

The LES sub-grid scale model used is the dynamic Smagorinsky model with local averaging. The low Mach number, incompressible Navier-Stokes equations are solved in a fully unstructured, node-based, finite-volume discretization based on a method developed by Ham (2007) [15]. The code used for FVM is the incompressible flow solver Cliff by Cascade Technologies Inc. A non-dimentional time step of $\Delta t = 0.1e-3$ was used to obtain fully converged results.

COMPUTATIONAL DOMAIN, GRID AND FLOW CONDITIONS

The Reynolds number based on diameter and average velocity in minimum area is 3000 in all simulations. The baseline configuration mimics the experiments of Ostanek and Thole [5]. A second configuration is the modification of the baseline configuration with a gap of $1D$ added above the pins. The motivation for using this configuration is to study the free end effects on the flow field and vortex dynamics of the pin array. The details of the geometry and the computational domain are introduced in the following sections. All the domains used in the simulations were meshed with fully unstructured hexahedral elements.

1. Baseline Geometry (No-Gap)

The geometry in experiments [5] is given by an array of staggered 9×7 circular pins of diameter D with an equilateral triangle pattern bounded between the two end-wallls. The streamwise and transverse spacings are $1.73D$ and $2D$, respectively, and the channel height is $1D$. The center of the first pin row is located $5D$ downstream from the inlet and the 7th pin row is located $10D$ upstream of the outlet of the channel. A schematic of the baseline geometry is shown in Figure 1. However, due to a reported symmetry of the flow in the center of the pin-fin array, the baseline simulations here are performed with periodic boundary conditions in a transverse direction for a single cylinder plus two half cylinders in the alternating rows, for the 7 rows of pins. Constant heat flux of one ($q'' = 1 units$) is imposed on all the pins and end-walls and a cold flow with zero temperature is injected in the inlet boundary. The mesh is clustered around pins and the end-walls, with a y^+ of 1 for the first grid point in the near wall region. Two different mesh counts of $1M$ (coarse mesh) and $8M$ (fine mesh) cells were used for the baseline geometry with no gap.

2. Geometry With Gap

The second geometry studied is the same geometry as the baseline geometry in 1 but with a free space added above the

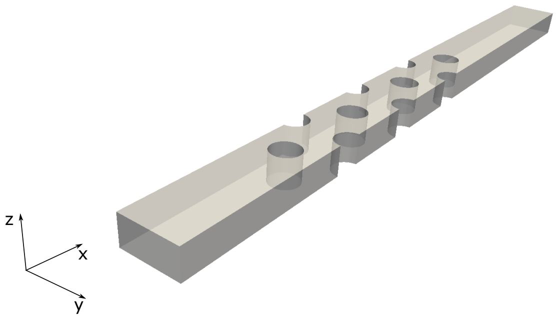

FIGURE 1: Computational domain of baseline geometry (No-Gap)

pins. This introduces additional flow complexity in terms of free-end three dimensional effects when compared to the no gap geometry. The top wall is at a height of $1D$ away from the top of the pin array as shown in Figure 2. A total mesh count of $2M$ cells was used for the gap configuration. The wall-normal y^+ value was maintained at 1 at all walls. Flow and boundary conditions are identical to that of the baseline geometry described previously.

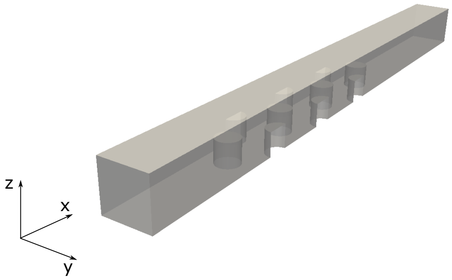

FIGURE 2: Computational domain of geometry with gap

SOLUTION VERIFICATION AND VALIDATION

In this section, details of a mesh refinement study are presented and discussed. In addition, mean velocity profiles at the first and third row wakes, wake closure positions and estimated frequency of vortex shedding at the first row are presented and compared with [5] for the baseline configuration with no gap.

Mesh Refinement study

Two different meshes are considered for the baseline no-gap configuration of Figure 1. First level of grid refinement is a mesh with 1M cells (coarse grid) and the second level of grid refinement consists of a mesh with 8M cells (fine grid). This will provide details of fine mesh compared to coarse mesh.

Mean Velocity Profiles

The time averaged mean stream-wise and transverse velocity profiles at the first row and third row wake for both SEM and FVM in comparison with the experimental data [5] are shown in Figures 3-4 for both coarse and fine grids. Uncertainties in LDV measurments are reported as 1.8% and 0.8% for mean stream-wise and span-wise velocities of [5] respectively. These uncertainties are calculated using a 1% bias uncertainty for instantaneous measurements in velocities. It should be noted that the experiment reports that the inflow is fully turbulent [5] using a sharp edge contraction between the plenum and the entry region to promote the flow unsteadiness [16]. However, at the channel Reynolds number used in the experiment ($Re_H = 1500$) the flow falls within the laminar regime which means that any disturbances in the inflow will die out through the inlet duct before reaching the first row. Consequently, for a consistent comparison, we have performed the simulations with inflow disturbances to try to emulate similar conditions to those of the experiment. For this purpose random perturbations with an intensity of 10% were added to the laminar inflow velocity profile for SEM. For FVM, the inlet velocity boundary condition uses stochastic inflow turbulence based on [17] generated with a turbulence intensity of 10%. Mesh refinement studies performed on the coarse mesh (1M) and a finer mesh (8M) on the mean velocity profiles at the wake of row 1 and row 3 pins show very little variation when increasing mesh size leaning towards the right trend relative to the experimental results. Furthermore, according to the velocity profile comparisons shown in in Figures 3-4, there exists a consistency between the different numerical methods used, justifying the need to circumvent the formal grid convergence index (GCI) study which requires a third, more expensive mesh (64M).

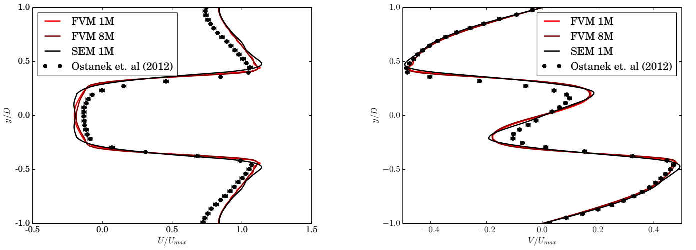

(a) Mean streamwise velocity profile

(b) Mean transverse velocity profile

FIGURE 3: Mean streamwise and transverse velocity profile at $\frac{x}{D} = 1D$ from pin center and, $\frac{z}{D} = 0.0$ for Row 1

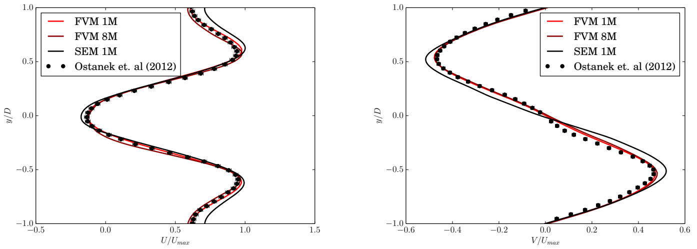

(a) Mean streamwise velocity profile (b) Mean transverse velocity profile

FIGURE 4: Mean streamwise and transverse velocity profile at $\frac{x}{D} = 1D$ from pin center and, $\frac{z}{D} = 0.0$ for Row 3

Frequency of Vortex Shedding

The frequency of the vortex shedding and the corresponding Strouhal number quantify LES results in comparison with experiments. One-dimensional energy spectrum is computed in the shear layer of the pin wake of the first row at a stream-wise distance of $\frac{x}{D} = 0.9$ and a transverse direction of $\frac{y}{D} = 0.4$ from the center of the pin. The peak frequency in the first row wake is shown in Table 1, along with the corresponding Strouhal number and the relative error in the Strouhal number compared to the experiment (e_{St}). As can be seen in Table 1 the estimated Strouhal frequency leaning towards the right trend relative to the experimental results with increasing the mesh counts from 1M to 8M.

TABLE 1: Errors in the calculation of Strouhal frequency in first row shear layer

Method	$f(Hz)$	$St = fD/U_{max}$	$e_{St}(\%)$
SEM (1M)	6.13	0.56	10.5
FVM (1M)	6.55	0.6	4.8
FVM (8M)	6.67	0.61	2.5
Experiment ([5])	6.84	0.63	–

Wake Closure Position

Another means of validating the simulations is by comparing the wake closure position ($\frac{L_r}{D}$) with the experiment. The wake closure position is defined as the position of zero time-mean stream-wise velocity along the wake axis. This is also referred to as the recirculating region. Table 2 shows the errors in wake closure position for both the methods. It can be seen that the relative errors for both SEM and FEM methods are less than 2% for both first and third row wakes. Again as can be seen in Table 2 the estimated wake closure position leaning towards the right trend relative to the experimental results by increasing the mesh counts from 1M to 8M.

TABLE 2: Relative errors in wake closure position ($\frac{L_r}{D}$) with respect to experimental data

Method	**Row 1**	e (%)	**Row 3**	e (%)
SEM (1M)	1.34D	1.47	1.15D	1.77
FVM (1M)	1.37D	0.74	1.14D	0.88
FVM (8M)	1.36D	0.0	1.14D	0.88
Experiment [5]	1.36D	–	1.13D	–

GUIDELINES FOR NUMERICAL SIMULATIONS

In this section, special considerations for performing simulations in pin-fin array geometries are discussed.

Significance of side wall effects

As described in the previous section, the validation of LES with experiment was conducted on a geometry with periodic boundary condition in transverse direction whereas [5] noted that the experimental measurements taken at the middle portion of the full channel are uninfluenced by wall effects. A study was performed to investigate whether this holds true for high-fidelity numerical simulations as well. The middle portion of the domain is at a distance $9D$ away from either side wall. Figure 5 shows the computational domain of the full baseline geometry with side walls in the transverse direction.

The mesh resolution for this case is identical to the periodic baseline geometry with 1M mesh resulting in a total mesh size of $9M$ mesh cells. No significant improvement in the time-averaged mean velocity due to the inclusion of the full geometry as compared to experimental data was noticed, thereby letting us to conclude that the use of periodic conditions in the transverse direction to reduce computational time is justified. An extension of this exercise is finding the distance from the side walls where its effect become negligible. Figures 6 - 7 show the normalized stream-wise velocities at various transverse locations within the channel from the side-wall to the center at $\frac{y}{D} = 0.0$.

It can be seen that at the distance of $4D$ from the side walls, the flow is no longer affected by wall effects. Hence good candidates for the location where the application of transverse periodic

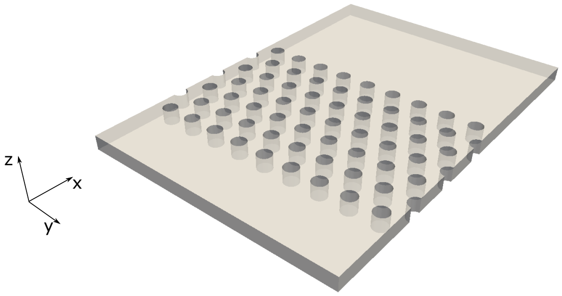

FIGURE 5: Computational domain of baseline geometry with transverse side walls

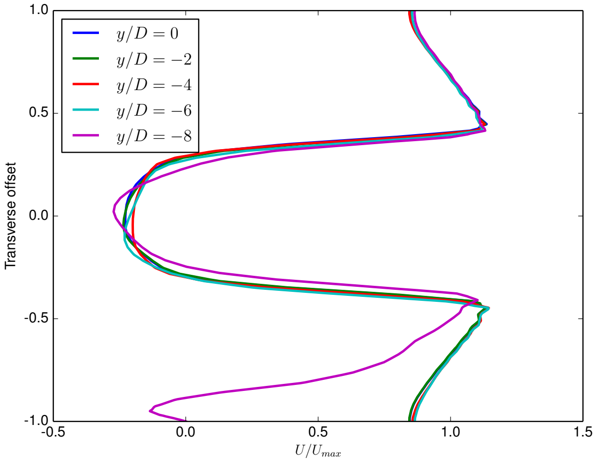

FIGURE 6: Stream-wise normalized mean velocity for row 1 wake at various transverse locations at $\frac{z}{D} = 0.0$, $\frac{x}{D} = 1D$ from pin center (FVM)

boundary conditions are valid, are pin 1 at a distance of $9D$ away from the side-walls.

Self similarity of fluid flow

It is often not feasible to perform high-fidelity simulations on large pin-fin arrays with high pin counts. One way of circumventing having to simulate the entire geometry is to apply periodic boundary conditions in both the stream-wise and transverse directions and drive the flow with a constant pressure gradient. We have investigated whether this assumption holds good and found that it is for the regions within the pin-fin array where the flow is predominantly affected by the vortices generated by the presence of the pin structures. In other words, beyond a certain stream-wise location within the pin-fin array, the flow becomes self-similar. The normalized stream-wise mean velocities at the wakes of different rows are shown in Figure 8. These simulations are performed using the full baseline geometry with side walls in the transverse direction.

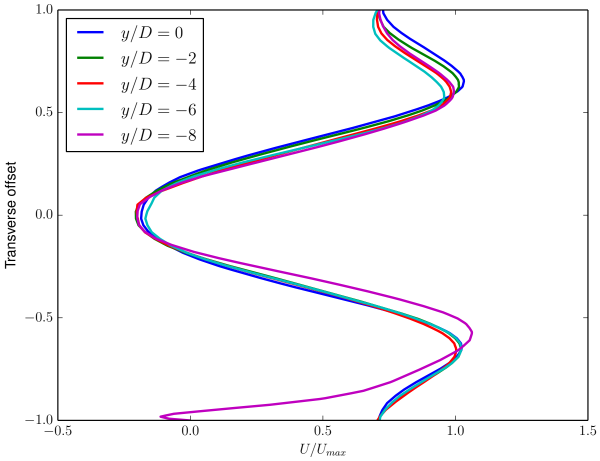

FIGURE 7: Stream-wise normalized mean velocity for row 3 wake at various transverse locations at $\frac{z}{D} = 0.0$, $\frac{x}{D} = 1D$ from pin center (FVM)

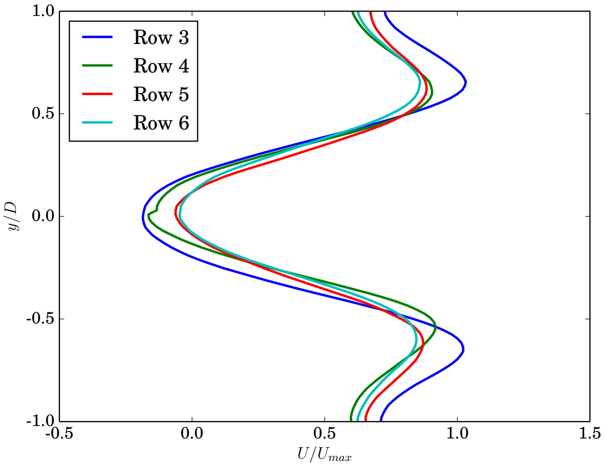

FIGURE 8: Stream-wise normalized mean velocity at different row wakes at $\frac{z}{D} = 0.0$, $\frac{x}{D} = 1D$ from pin center (FVM)

The time-averaged velocities show that beyond row 4, the velocities begin to become self-similar and show a good match with the velocity profiles of further rows. Stream-wise periodic boundary conditions thus appear valid for pins in row 5 and beyond.

ANALYSIS OF 3D FLOW PHYSICS

We focus now on the analysis of the flow field and thermal field pattern and their correlation with the vortex structures.

Mean Velocity Profiles

The normalized mean velocity profiles at the wake regions as described in previous sections provides a comprehensive picture of the time-averaged flow velocities along the mid-plane of the domain. In this section, the time-averaged flow velocity profiles along the length of the pins at varying transverse directions are discussed. This aims to provide an understanding of how the flow physics contrasts especially when comparing the baseline geometry with the baseline geometry with gap.

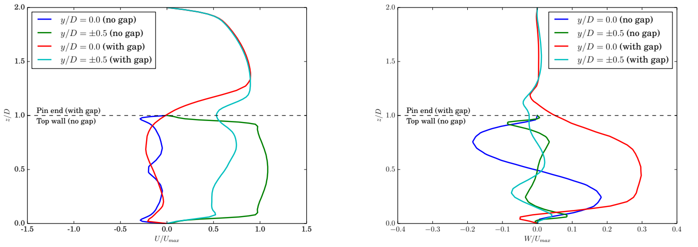

(a) Stream-wise normalized mean velocity (b) Span-wise normalized mean velocity

FIGURE 9: Mean normalized velocity profile for row 1 wake along the mid-plane at $\frac{x}{D} = 1D$ from pin center (FVM)

The stream-wise location of the profiles is the same as that of the mid-plane velocity profiles for the baseline geometry. Figures 9-10 show the stream-wise and span-wise mean velocity components at a location along the mid-span of the channel which is $\pm 0.5D$ away from the mid-span of the channel. High gradients of stream-wise velocity are observed directly behind the first row along the length of the pin. This behavior is not observed moving along the transverse direction. The gradients of stream-wise velocity directly downstream of the pin along the pin height are relatively less extreme for the baseline geometry with gap, as observed in Figures 9 and 10. These gradients in stream-wise velocity are noticeable even when moving a distance 0.5 D along the transverse direction, due to the interaction of the unobstructed flow above the pin and the flow downstream of the pin tip itself. The flow directly downstream of the pin is towards the unobstructed region of the geometry as evidenced by the large contribution of the longitudinal velocity shown in Figures 9 and 10, although the effect seemingly decays when moving away from the pin along the transverse direction. The normalized time averaged mean velocity profiles with respect to U_{max} at first and third row wakes are compared with the results presented in the previous section. This aims to provide an understanding of how the flow physics and wake behaviour differ comparing the baseline geometry with gap and without any gap. Figure 11 shows the time-averaged mean stream-wise velocities in the pin half height plane ($\frac{z}{D} = 0.0$ for the geometry with no gap, and $\frac{z}{D} = -0.5$ for the geometry with gap). The stream-wise location of the profiles is the same as that of the mid-plane velocity profiles for the baseline geometry. A noticeable reduction in the strength of the recirculation region is observed in the third row wake for the geometry with gap in comparison with the geometry without gap. This is due to the fact that the approaching flow above the pin re-attaches on the free end for the third row. However, this is not the case considering the flow above the free end in the first row. Time averaged streamlines in the mid-plane are shown for both geometries in Figure 12, illustrating this effect. The overall comparison of the wake at both locations also shows very small changes in the width of the wake region for both first and third rows.

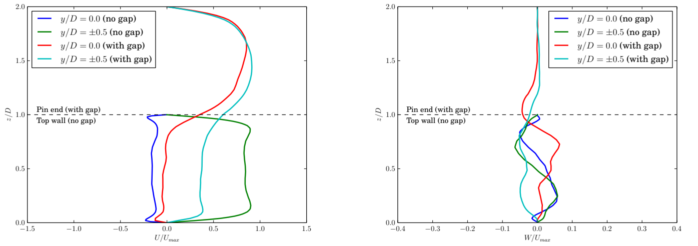

(a) Stream-wise normalized mean velocity (b) Span-wise normalized mean velocity

FIGURE 10: Mean normalized velocity profile for row 3 wake along the mid-plane at $\frac{x}{D} = 1D$ from pin center (FVM)

Horseshoe Vortex Dynamics

In this section the evolution of the horseshoe vortex system in different rows and its effect on the heat transfer is presented and analyzed. Wall resolved LES reveals a broad spectrum of scales, as illustrated in Figure 13 for both geometries by iso-contours of λ_2 vortices coloured by mean stream-wise velocity. These plots along with the iso-contours of λ_2 vortices in the $z = -0.48$ plane shown in Figure 14 and time-averaged streamlines (Figure 12) superimposed on the temperature field in the mid-plane cutting through pins 1 and 3 indicate the presence of the horseshoe vortex in different rows. However, the interacting vortex system including: HV, SV, TV shown by Hunt et al. [1] at the pin and end-wall junction is only present in the first row.

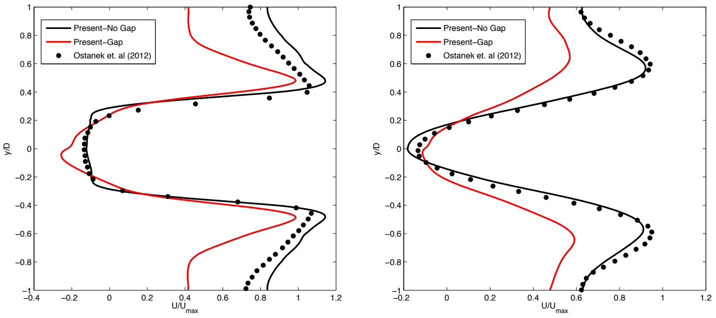

(a) Row 1 (b) Row 3

FIGURE 11: Stream-wise normalized mean velocity at $\frac{x}{D} = 1D$ from pin center (No-gap $\frac{z}{D} = 0.0$, gap $\frac{z}{D} = -0.5$) (SEM)

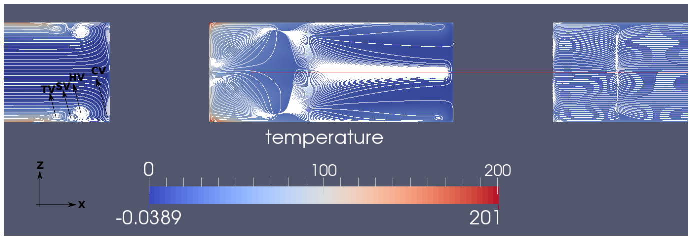

(c) geometry with no gap

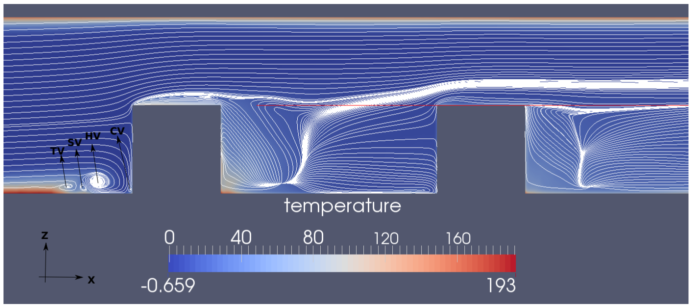

(d) geometry with gap

FIGURE 12: Time averaged streamlines superimposed on temperature contour at $\frac{y}{D} = 0$ plane (SEM)

From the first row onward the primary horseshoe vortex is the only vortex structure that can be seen at the pin and end-wall junction. It is of interest to see how these vortices will affect the temperature. High temperature values in Figure 15 in the regions at which the horseshoe vortex is present also show that the horseshoe vortex contributes to the end-wall heat transfer. As can be seen from the temperature contours the contribution of the horseshoe vortex system in the first and second rows is more pronounced in comparison with the other rows. This is due to the fact that the horseshoe vortex is much stronger in the upper rows which can also be seen in Figures 12. In the mid-plane, however, periodic unsteadiness (KV) is the primary mechanism for heat transfer (see Figure 16). As the flow goes through the array there is an increase in the flow temperature that represents the gradual heating of the flow by the heat added through the pins and end-walls.

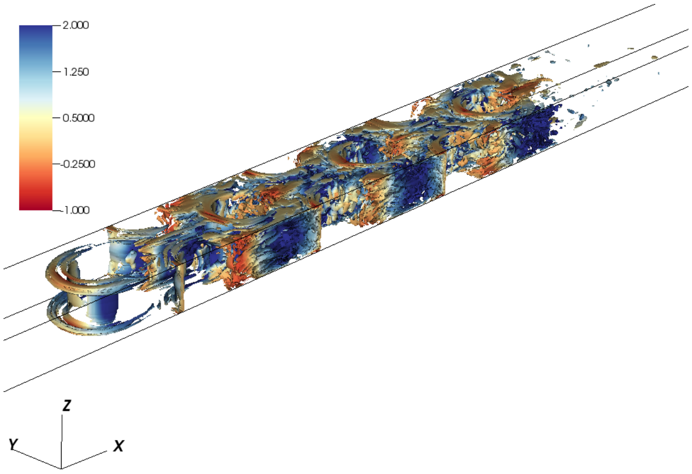

(a) geometry with no gap

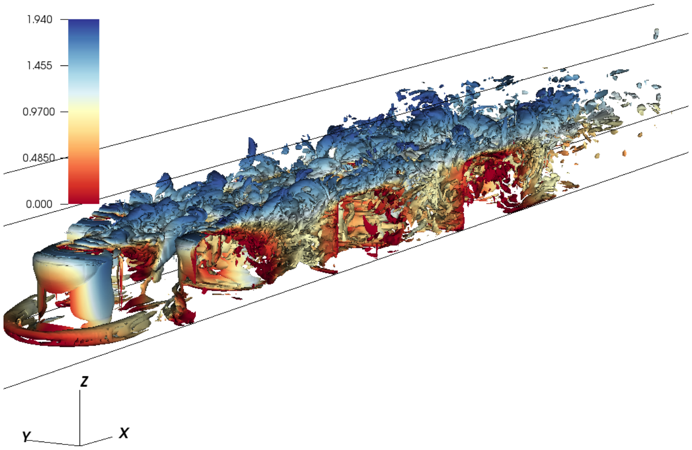

(b) geometry with gap

FIGURE 13: Iso-contours of λ_2 vortices coloured with time-averaged stream-wise velocity (SEM)

Comparison of countors of mean temperature at $\frac{y}{D} = 0$ plane shown in Figure 17 reveals that the horseshoe vortex at the first pin row is more compact and vigorous for the geometry with gap in comparison with the baseline geometry with no gap. Inspection of Figure 17 indicates that the hosrseshoe vortex extends further from the pin end-wall junction both in stream-wise and transverse directions for the the baseline geometry with gap.

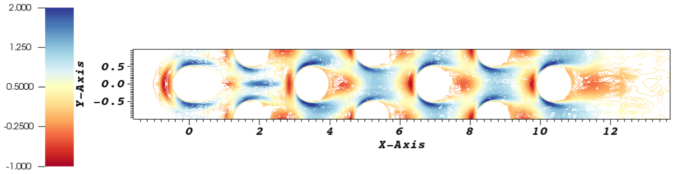

FIGURE 14: Iso-contours of λ_2 vortices for baseline geometry with no gap coloured with time-averaged stream-wise velocity in $\frac{z}{D} = -0.48$ plane (SEM)

This can be also verified from the contours of mean temperature shown in Figure 18 at a distance of 0.15 from the lower wall, in which a greater extent of high temperature can be found around the pin surface and at the pin end-wall junction in the first row. This is due to the fact that for the geometry with gap the horseshoe vortex has enough space to grow, however it is more confined due to the presence of the upper wall for the geometry without gap.

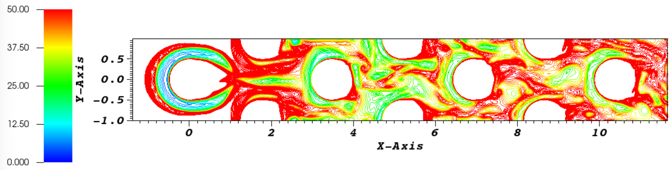

FIGURE 15: Iso-contours of instantaneous temperature for the geometry with no gap in $\frac{z}{D} = -0.48$ plane (SEM)

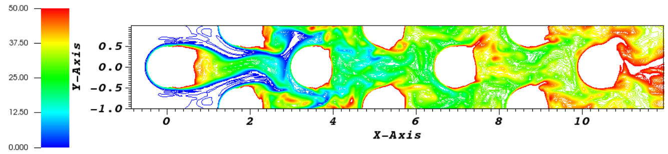

FIGURE 16: Iso-contours of instantaneous temperature for the geometry with no gap at the channel half height, $\frac{z}{D} = 0.0$ (SEM)

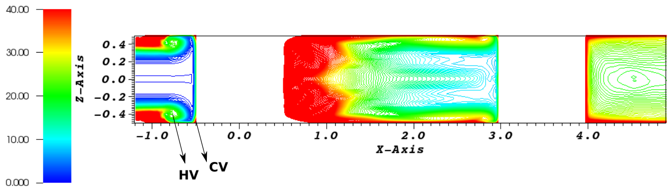

(a) geometry with no gap

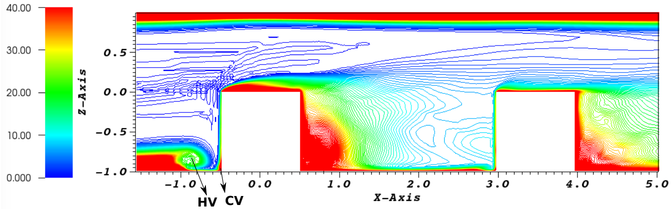

(b) geometry with gap

FIGURE 17: Iso-contours of mean temperature at $\frac{y}{D} = 0$ plane (SEM)

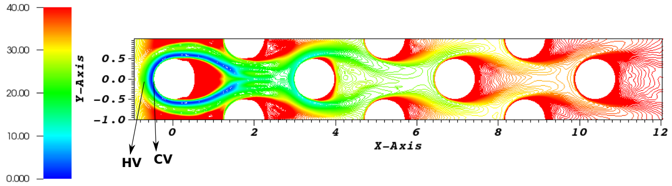

(a) geometry with no gap

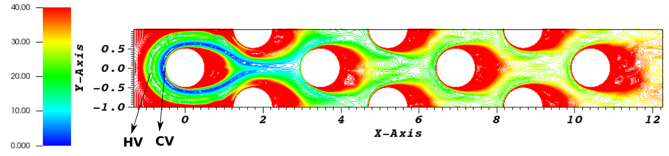

(b) geometry with gap

FIGURE 18: Iso-contours of mean temperature at $\frac{\Delta z}{D} = 0.15$ above the lower wall (SEM)

CONCLUSION

Results of large eddy simulations of flow through a staggered array of pin-fins with and without gap using two different numerical approaches are analyzed and compared. The study presented confirms the results reported in previous studies and also sheds more light on the mean flow, complex three dimensional structures and the instantaneous flow features. The simulations have been validated against experiments from literature as well as verified with grid refinement. Numerical simulations performed including the effect of side-walls show no significant change in the time-averaged mean velocities as compared to simulating the center with periodicity, thereby showing the feasibility of using periodic boundary conditions at domain side boundaries for the purpose of reducing computational cost. The comparison of the stream-wise normalized velocities at different row wakes show that starting with the fifth row the velocities begin to become self-similar. This indicates the suitability of applying stream-wise periodic boundary conditions for studying the flow dynamics in fourth and beyond. The stream-wise and transverse mean velocities show a high gradient of velocity behind the first row along the length of the pin. The stream-wise mean velocity of the first and third row wakes between the baseline geometries with and without gap show a noticeable reduction in the third row wake for the baseline geometry with gap which is due to reattachment of the flow above the pin surface. The analysis of the horseshoe vortex dynamics also shows that the horseshoe vortex is present at all rows at the pin and end-wall junction. However, it is much stronger in the first and second rows of the array. The instantaneous contours of temperature at the near wall region show a significant contribution of the horseshoe vortex to the end-wall heat transfer, especially in the initial rows. Furthermore, comparison of contours of mean temperature for the two geometries reveals that the horseshoe vortex at the base is more vigorous and greater in size for the geometry with gap than the one without gap.

ACKNOWLEDGMENT

The numerical work reported here has been funded by AORA Solar Ltd. The authors would like to thank the support of Arizona State University for providing compute allocations.

Reference

[1] J. C. R. Hunt, C. J. Abell, and J. A. Peterka. Kinematical studies of the flows around free or surface mounted obstacles; applying topology to flow visualization. *J. Fluid Mechanics*, 86:179–200, 1978.

[2] T. J. Praisner, C. V. Seal, L. Takmaz, and C. R. Smith. Spatial-temporal turbulent flow-field and heat transfer behavior in end-wall junctions. *Int J. Heat Fluid Flow*, 18:142–151, 1997.

[3] F. E. Ames, C. A. Nordquist, and L. A. Klennert. Endwall heat transfer measurements in a staggered pin-fin array with an adiabatic pin. ASME Paper No. GT2007-27432, 2007.

[4] J. K. Ostanek. *Flow-Field Interactions In Low Aspect Ratio Pin-Fin Arrays*. PhD Thesis, The Pennsylvania State University, May 2012.

[5] J. K. Ostanek and K. A. Thole. Wake development in staggered short cylinder arrays within a channel. *Journal of Experiments in Fluids*, 53:673–697, 2012.

[6] F. E. Ames and L. A. Dvorak. Turbulent transport in pin-fin arrays: Experimental data and predictions. *Journal of Turbomachinery*, 128:71–81, 2006.

[7] G. Delibra, K. Hanjalic D. Borello, and F. Rispoli. Vortex structures and heat transfer in a wall-bounded pin matrix: LES with a RANS wall-treatment. *International Journal of Heat and Fluid flow*, 31:740–753, 2010.

[8] G. P. Salvador, T. Stoesser, and J. Frohlich. Large eddy simulation and experiments of flow around finite height cylinders. *Journal of Flow Turbulence Combustion*, 84:239–275, 2010.

[9] E. M. Sparrow and J. W. Ramsey. Heat transfer and pressure drop for a staggered wall attached array of cylinders with tip clearance. *International Journal of Heat and Mass Transfer*, 21:1369–1377, 1978.

[10] M. Deqing, L. Xinyang, and M. Qian. Effect of tip clearance on the heat transfer and pressure drop performance in the micro-reactor with micro-pin-fin arrays at low Reynolds number. *International Journal of Heat and Mass Transfer*, 70:709–718, 2014.

[11] K. A. Moores and Y. K. Joshi. Effect of tip clearnace on the thermal and hydrodynamic performance of a shrouded pin fin array. *Journal of Heat Transfer*, 125:999–1006, 2003.

[12] E. M. Sparrow, B. R. Baliga, and S. V. Patankar. Forced convection heat transfer from a shrouded pin-fin array with and without tip clearance. *ASME Journal of Heat Transfer*, 100:572–579, 1978.

[13] R. A. Wirtz, W. Chen, and R. Zhou. Effect of flow bypass on the performance of longitudinal fin heat sinks. *ASME Journal of Electron Package*, 116:206–211, 1994.

[14] J. W. Lottes P. F. Fischer and S. G. Kerkemeier. Nek5000 web page. http://nek5000.mcs.anl.gov, 2008.

[15] F. Ham. An efficient scheme for large eddy simulation of low mach combustion in complex configurations. Annual Research Briefs, Center for Turbulence Research, Stanford University, 2007.

[16] J. K. Ostanek and K. A. Thole. Personal communication, 2015.

[17] S. Lee, S. Lele, and P. Moin. Simulation of spatially evolving compressible turbulence and the application of taylors hypothesis. *Journal of Physics of Fluids*, 4:1521–1530, 1992.